

## Research on dynamic modeling and carbon load estimation of diesel particulate filter

Dongwei Yao, Jiadong Hu, Benxi Zhang, Yihe Zhang & Feng Wu

**To cite this article:** Dongwei Yao, Jiadong Hu, Benxi Zhang, Yihe Zhang & Feng Wu (2023) Research on dynamic modeling and carbon load estimation of diesel particulate filter, Energy Sources, Part A: Recovery, Utilization, and Environmental Effects, 45:4, 12165-12180, DOI: [10.1080/15567036.2023.2269126](https://doi.org/10.1080/15567036.2023.2269126)

**To link to this article:** <https://doi.org/10.1080/15567036.2023.2269126>



Published online: 25 Oct 2023.



Submit your article to this journal [↗](#)



Article views: 93



View related articles [↗](#)



View Crossmark data [↗](#)



# Research on dynamic modeling and carbon load estimation of diesel particulate filter

Dongwei Yao<sup>a,b</sup>, Jiadong Hu<sup>a</sup>, Benxi Zhang<sup>a</sup>, Yihe Zhang<sup>a</sup>, and Feng Wu<sup>a</sup>

<sup>a</sup>College of Energy Engineering, Zhejiang University, Hangzhou, China; <sup>b</sup>Key Laboratory of Smart Thermal Management Science & Technology for Vehicles of Zhejiang Province, Zhejiang Yinlun Machinery Company, Taizhou, China

## ABSTRACT

Accurate estimation of carbon load in diesel particulate filters is an important basis for efficient and safe operation of active regeneration. Currently, model-based carbon load prediction has the advantages of high accuracy and low influence by working conditions. In this paper, a dynamic model of diesel particulate filters was developed based on the deep bed and cake layer trapping mechanism and regeneration mechanism. The trapping process was described using the spherical trapping mechanism, while the regeneration process was based on the non-catalytic oxidation process of the trapped particles. A pressure drop correction based on the extended Kalman filter was developed to correct the errors accumulated in the carbon load prediction during the integration. The maximum error of carbon load prediction was 0.3 g/L, and the average error was less than 0.17 g/L, the maximum error of pressure drop was 0.7 kPa, and the average error was less than 0.33 kPa. The carbon load prediction algorithm was proved to have good accuracy and can be used for start-stop judgment of DPF active regeneration, and the pressure drop and temperature calculated by the DPF model can be used for DPF status monitoring during regeneration to ensure safety and reliability.

## ARTICLE HISTORY

Received 22 May 2023  
Revised 28 August 2023  
Accepted 22 September 2023

## KEYWORDS



DPF; model; carbon load estimation; pressure drop; particle

## Introduction

Diesel vehicles emit 80% of NO<sub>x</sub> and more than 90% of Particulate Matter(PM) from automobiles (Reşitoğlu, Altinişik, and Keskin 2015), which is a serious hazard to the human heart, lungs, and other tissues (Jin, Tian, and Tong 2016). PM emissions from diesel engines have become a global problem that needs to be addressed urgently (Sun, Cai, and Zhao 2021).

Diesel Particulate Filter(DPF) is the main way to remove particles from diesel exhaust (Bin et al. 2015). After DPF traps a certain degree of carbon particles, the exhaust pressure increases and DPF needs to be regenerated. The regeneration method is divided into active regeneration and passive regeneration. The passive regeneration rate is slow and the temperature window is generally between 300–400°C (Rossomando et al. 2019). Active regeneration heats the airflow at the DPF inlet to about 600°C to heat the particles in the DPF to the ignition temperature (Bai et al. 2016a). Active regeneration is an issue not only for uncoated DPFs but also for catalytic DPFs. Specifically, in the case of catalytic DPFs, fast and, at the same time, low-temperature regeneration is not possible (Di Sarli and Di Benedetto 2015, 2016, 2018), unless the accumulation of particles in the form of a cake layer on top of the filter walls is prevented (Di Sarli and Di Benedetto 2018, 2019; Landi, Di Sarli, and Lisi 2021).

The timing of the active regeneration trigger affects the safety and economy of the engine. Too early regeneration leads to increased fuel consumption, and too late regeneration leads to high exhaust back

**CONTACT** Dongwei Yao  [dwyao@zju.edu.cn](mailto:dwyao@zju.edu.cn)  College of Energy Engineering, Zhejiang University, 38 Zheda Road, West Lake District, Hangzhou, Zhejiang Province 310027, China

This article has been corrected with minor changes. These changes do not impact the academic content of the article.

© 2023 Taylor & Francis Group, LLC

pressure and can even be dangerous (Shi et al. 2019). Therefore, rational control of DPF regeneration is needed to improve fuel economy and extend service life. The key indicator for determining the initiation of regeneration is carbon load.

It is difficult to directly measure the carbon load in real time because of the complex phenomena in the DPF. There are three main methods to estimate the carbon load. The first method uses additional equipment or sensors (Feulner et al. 2017; Kort et al. 2021). However, this method increases the cost and does not significantly improve the prediction accuracy. The second method is based on the calculation of pressure drop. The relationship between pressure drop, exhaust temperature, and carbon load is established (Du et al. 2018; Shi et al. 2020). This is the most commonly used method for calculating carbon load, but the data estimated by this method has an error of 4 ~ 6 g with experimental measurements (Ran et al. 2018).

The third method is a model-based prediction method. Tang (Bai et al. 2016b; Tang et al. 2015) developed a DPF particle loading model consisting of a transient emission model of particles and a model of particle oxidation to compensate for the large deviation of the DPF pressure drop sensor at low exhaust flow rates. Huang (Huang et al. 2019) developed an empirical model of diesel engine NO<sub>x</sub> and particle mass emissions to assist in estimating the carbon load of diesel engines, modeled the particle oxidation rate in DPF based on the catalytic particle oxidation reaction mechanism, and proposed an online observation method of the carbon load of DPF based on the mass balance. These models of particle emission reduce the need for particle emission testing but do not take into account that there is a relationship between the particle emitted by the engine and the particle trapped in the DPF in terms of trapping efficiency.

Chiavola (Chiavola, Chiatti, and Sirhan 2019) built a DPF model based on the “unit-collector” and hydrodynamic methods. The model was used to predict the change of trapped particle mass and back pressure with time as the particle size varied during the loading process, and to study the effect of particle size on back pressure. Wang (Wang et al. 2021) proposed a new carbon load prediction model based on the collection mechanism and multilayer equivalent permeability considering the deep bed and cake layer collection. Tan (Tan et al. 2020) introduced a variable effective density parameter to modify the filter model and a global filtration correction factor  $\vartheta_p$  that took into account the variation of particle morphology parameters, and the prediction accuracy of the extended model was improved by 34.08% compared to the original model. These studies focused on the prediction of particles in the trapping phase and the effect on pressure drop, and the accuracy of the models was improved by introducing parameters such as particle diameter.

Zhang (Zhang et al. 2020) considered ash deposition in the deep bed and filter cake in an existing carbon load prediction model, and added a fuzzy adaptive variable weight function linked neural network model and a cusp catastrophe model to predict the endpoints of carbon load for different fuels and initial ash masses.

Lao (Lao et al. 2019) developed a new model to describe transient PM and Particle Number (PN) emissions during the active regeneration experiment of DPF. As emissions regulations become more stringent, particle emissions during active DPF regeneration will be of increasing concern. Zhong (Zhong et al. 2022) developed a DPF passive-active coupled regeneration model to investigate the regeneration state and temperature boundaries in the passive-active composite coupled regeneration process. Depcik (Depcik, Langness, and Mattson 2014) developed a lumped DPF model for the Electronic Control Unit (ECU). The model formulation was simplified based on standard control equations to eliminate computational overhead. However, the model employed incompressibility assumptions to remove the interdependence of the ideal gas law, resulting in larger errors between the calculated pressure drop and components compared to the standard compressible flow versions of the literature.

In summary, some carbon load prediction methods need to be equipped with additional equipment, which increases the cost and does not significantly improve the prediction accuracy, while pressure drop-based carbon load prediction suffers from the problem of being affected by sudden changes in operating conditions. The model-based carbon load prediction in the literature has high accuracy but also has a large computational burden, which is not suitable for real-time control of DPF regeneration on real vehicles.

Therefore, to obtain carbon load prediction that can be used for real-time control of DPF regeneration in real vehicles, a simpler 0-dimensional DPF model was adopted, and a dynamic model of DPF was constructed using a “unit-collector” model and particle non-catalytic oxidation regeneration reaction.

The error generated by the model iteration accumulates over a long period, so an Extended Kalman Filter(EKF) was designed to correct the accumulating error, and data such as carbon load and DPF temperature can be provided to develop a reasonable regeneration strategy. The model was verified by bench test with high accuracy and can be used for real-time control of DPF active regeneration.

## Diesel particulate filter dynamic modeling

### Particle trapping modeling

The main assumptions of the model are: 1. the DPF inlet gas properties are spatially homogeneous; 2. the gas volume is incompressible; 3. the distribution of particles within the DPF is not considered, and the particles are considered to be uniformly accumulated within the DPF pores and on the walls.

The trapping process of wall flow DPF mainly includes the deep bed trapping process and the cake layer trapping process. At the early stage of trapping, particles are trapped by the porous wall of DPF, and as the trapping proceeds, the particles gradually turn to accumulate on the surface layer of the porous wall, and the cake layer particle formed by accumulation become a new porous structure and continue to trap particles.

Deep bed trapping section, the spherical trapping mechanism (Chiavola et al. 2020) is used to calculate the trapping efficiency of the porous structure. The trapping process of particles in a real porous medium can be approximated as the trapping process on the surface of a spherical trapping unit. Three mechanisms, direct interception, Brownian diffusion, and inertial collision, are used to describe the trapping process, and among the three mechanisms, Brownian diffusion and direct interception play a dominant role while inertial collision can be neglected (Chiavola et al. 2020).

It is generally considered that when particles are trapped by one mechanism and then no longer trapped by other mechanisms, the integrated trapping factor is calculated as follows:

$$\eta_{DR} = \eta_D + \eta_R - \eta_D \eta_R \quad (1)$$

$\eta_{DR}$  is the integrated trapping factor,  $\eta_D$  is the Brownian diffusion factor, and  $\eta_R$  is the direct interception factor. After obtaining the integrated trapping factor, the deep bed trapping efficiency is calculated as follows (Wang 2013):

$$E_{dep} = 1 - \exp \left[ -\frac{3\eta_{DR}(1-\varepsilon)w_{wall}}{2\varepsilon d_{dep}} \right] \quad (2)$$

$E_{dep}$  is deep bed trapping efficiency,  $\varepsilon$  is the porosity of the porous wall,  $w_{wall}$  is the wall thickness of DPF, and  $d_{dep}$  is the diameter of the deep bed trapping unit.

The Brownian diffusion factor can be calculated as follows (Chiavola et al. 2020):

$$\eta_D = 3.5g(\varepsilon)Pe^{-\frac{2}{3}} \quad (3)$$

$$g(\varepsilon) = \left[ \frac{\varepsilon}{2-\varepsilon-\frac{9}{5}(1-\varepsilon)^{\frac{1}{3}}-\frac{1}{5}(1-\varepsilon)^2} \right]^{\frac{1}{3}} \quad (4)$$

$g(\varepsilon)$  is the pore function changed with the porosity, and  $Pe$  is the Peclet number.

$$Pe = \frac{Ud_{dep}}{D_p} \quad (5)$$

$$U = \frac{u_w}{\varepsilon} \quad (6)$$

$$D_p = \frac{k_B T_w}{3\pi\mu_g d_p} \quad (7)$$

$U$  is the flow rate in the pore,  $D_p$  is the diffusion coefficient of particles in the pore,  $u_w$  is wall flow velocity;  $k_B$  is Boltzmann constant;  $T_w$  is the wall temperature,  $\mu_g$  is air viscosity,  $d_p$  is the average diameter of particles.

The direct interception factor can be calculated as follows (Depcik, Langness, and Mattson 2014):

$$\eta_R = 1.5N_R^2 \frac{g(\varepsilon)^3}{(1+N_R)^{\frac{3-2\varepsilon}{3\varepsilon}}} \quad (8)$$

$$N_R = \frac{d_p}{d_{\text{dep}}} \quad (9)$$

$N_R$  is the interception parameter.

It is assumed that the captured particles are uniformly distributed on the trapping unit. The deep bed trapping unit diameter and porosity will change with the accumulation of particles and the following equations are given to update the deep bed trapping unit diameter and porosity with the trapped mass:

$$\varepsilon = 1 - \frac{\pi d_{\text{dep}}^3}{3b_{\text{dep}}^3} \quad (10)$$

$$d_{\text{dep}} = \left[ d_{\text{dep}0}^3 + \left( \frac{6m_{\text{dep}}}{n_{\text{dep}}\rho_{\text{particle,dep}}\pi} \right) \right]^{\frac{1}{3}} \quad (11)$$

$$d_{\text{dep}0} = \frac{3(1-\varepsilon_0)d_{\text{pore}}}{2\varepsilon_0} \quad (12)$$

$$b_{\text{dep}} = d_{\text{dep}0} \sqrt[3]{\frac{\pi}{3(1-\varepsilon_0)}} \quad (13)$$

$b_{\text{dep}}$  is the side length of deep bed trapping unit,  $d_{\text{dep}0}$  is the initial diameter of deep bed trapping unit,  $m_{\text{dep}}$  is particle mass trapped in deep bed layer,  $n_{\text{dep}}$  is the number of trapping units in deep bed layer,  $\rho_{\text{particle,dep}}$  is particle density in deep bed layer,  $d_{\text{pore}}$  is average pore diameter,  $\varepsilon_0$  is initial porosity of the porous wall.

Cake layer trapping section, the splitting factor was used to describe the share of cake layer trapping in the trapping process (Tang et al. 2015).

$$\begin{aligned} \varphi_{\text{cut}} &= \frac{E_{\text{cake}}}{E_{\text{sum}}} \\ &= \frac{E_{\text{cake}}}{E_{\text{cake}} + (1 - E_{\text{cake}})E_{\text{dep}}} \end{aligned} \quad (14)$$

$\varphi_{\text{cut}}$  is a splitting factor.

Therefore, the cake layer trapping efficiency can be calculated by the deep bed trapping efficiency and the splitting factor:

$$E_{\text{cake}} = \frac{\varphi_{\text{cut}}E_{\text{dep}}}{1 + \varphi_{\text{cut}}E_{\text{dep}} - \varphi_{\text{cut}}} \quad (15)$$

$$\varphi_{\text{cut}} = \frac{d_{\text{dep}}^2 - d_{\text{dep}0}^2}{(\varphi b_{\text{dep}})^2 - d_{\text{dep}0}^2} \quad (16)$$

$\varphi$  is the dimensionless accumulation correction factor which reflects the carbon loading corresponding to the turning point of deep bed trapping to cake layer trapping,

### Particulate regeneration modeling

The chemical reactions that occur during the regeneration of the particle mainly involve the oxidation of carbon particles to carbon dioxide. The oxidation of particles by NO<sub>2</sub> and the reaction of other particle components are ignored.

The regeneration reaction rate of carbon particles can be calculated by the Arrhenius equation. The equations for the oxidation rate of carbon particles in the cake layer and deep bed layer are shown below. :

$$R_{\text{cake}} = m_{\text{cake}} C_{\text{O}_2} A_c \exp\left(-\frac{E_c}{R_g T_w}\right) \quad (17)$$

$$R_{\text{dep}} = m_{\text{dep}} C_{\text{O}_2} A_c \exp\left(-\frac{E_c}{R_g T_w}\right) \quad (18)$$

$R_{\text{cake}}$  and  $R_{\text{dep}}$  are the cake layer particle regeneration rate and the deep bed layer particle regeneration rate,  $m_{\text{cake}}$  is particle mass trapped in the cake layer,  $C_{\text{O}_2}$  is oxygen concentration in the reaction layer,  $A_c$  is pre-exponential factor of the particle oxidation,  $E_c$  is activation energy of particle oxidation reaction,  $R_g$  is universal gas constant,  $T_w$  is wall temperature of DPF.

In addition, the oxidation reaction of unreacted hydrocarbons(HC) within the Diesel Oxidation Catalyst(DOC) into the DPF during regeneration was also considered according to (Wu et al. 2019):

$$R_{\text{HC}} = b_{\text{pt}} w_{\text{wall}} C_{\text{O}_2} C_{\text{HC}} A_{\text{HC}} \exp\left(-\frac{E_{\text{HC}}}{RT_w}\right) \quad (19)$$

$R_{\text{HC}}$  is the rate of reaction of gaseous hydrocarbons in the DPF,  $b_{\text{pt}}$  is the amount of catalyst coating of DPF,  $C_{\text{HC}}$  is the molar fraction of hydrocarbons in the DPF,  $A_{\text{HC}}$  is the pre-exponential factor of the reaction, and  $E_{\text{HC}}$  is the activation energy of the reaction.

### Temperature modeling

The equations for conservation of energy for the upstream and downstream gas phases are

$$c_{p,g1} \rho_{g1} n_{\text{in}} w_{\text{ch,in}}^2 l_{\text{DPF}} \frac{\partial T_{g1}}{\partial t} = \dot{m}_{\text{exh}} c_{p,g1} T_{\text{in}} - \dot{m}_{\text{exh}} c_{p,g1} T_{g1} + 4n_{\text{in}} w_{\text{ch,in}} l_{\text{DPF}} h_1 (T_w - T_{g1}) \quad (20)$$

$$c_{p,g2} \rho_{g2} n_{\text{out}} w_{\text{ch,out}}^2 l_{\text{DPF}} \frac{\partial T_{g2}}{\partial t} = \dot{m}_{\text{exh}} c_{p,g1} T_{g1} - \dot{m}_{\text{exh}} c_{p,g2} T_{g2} + 4n_{\text{out}} w_{\text{ch,out}} l_{\text{DPF}} h_2 (T_w - T_{g2}) \quad (21)$$

$c_{p,g}$  is specific heat at constant pressure of gas phase,  $\rho_g$  is gas density,  $T_g$  is gas phase temperature,  $h$  is the heat transfer coefficient between the gas-solid phases, the index 1 represents the upstream channels, and the index 2 represents the downstream channels,  $T_{\text{in}}$  is DPF inlet gas flow temperature.

Chemical reactions are thought to take place in the solid phase and directly affect the solid phase temperature. The equation for conservation of energy in the solid phase satisfies:

$$c_{p,\text{DPF}} m_{\text{DPF}} \frac{\partial T_w}{\partial t} = A_1 h_1 (T_{g1} - T_w) + A_2 h_2 (T_{g2} - T_w) + \Delta H_C (A_1 R_{\text{cake}} + A_2 R_{\text{dep}}) + \Delta H_{\text{HC}} A_2 R_{\text{HC}} + \pi D_{\text{DPF}} l_{\text{DPF}} h_{\text{amb}} (T_{\text{amb}} - T_w) \quad (22)$$

$$A_1 = 4n_{\text{in}} w_{\text{ch,in}} l_{\text{DPF}} \quad (23)$$

$$A_2 = 4n_{\text{out}} w_{\text{ch,out}} l_{\text{DPF}} \quad (24)$$

$c_{p,\text{DPF}}$  is the specific heat at a constant pressure of DPF,  $m_{\text{DPF}}$  is the mass of DPF,  $\Delta H_C$  is the enthalpy change of particle oxidation,  $\Delta H_{\text{HC}}$  is the enthalpy change of HC,  $D_{\text{DPF}}$  is the diameter of DPF,  $h_{\text{amb}}$  is the heat transfer coefficient of DPF and environment, and  $T_{\text{amb}}$  is the temperature of the environment.  $A_1$  and  $A_2$  are heat transfer areas of upstream and downstream channels.

### Carbon load accumulation modeling

The mass conservation equations for cake layer trapping and deep bed trapping are:

$$\frac{dm_{\text{cake}}}{dt} = E_{\text{cake}} \frac{\dot{m}_{\text{exh}}}{\rho_{\text{exh}}} C_{\text{particle}} - A_1 M_{\text{particle}} R_{\text{cake}} \quad (25)$$

$$\frac{dm_{\text{dep}}}{dt} = E_{\text{dep}} (1 - E_{\text{cake}}) \frac{\dot{m}_{\text{exh}}}{\rho_{\text{exh}}} C_{\text{particle}} - A_2 M_{\text{particle}} R_{\text{dep}} \quad (26)$$

$\dot{m}_{\text{exh}}$  is the mass flow of the exhausted gas,  $\rho_{\text{exh}}$  is the density of exhaust gas,  $C_{\text{particle}}$  is the particle concentration of exhaust gas,  $M_{\text{particle}}$  is the molar mass of particle,  $n_{\text{in}}$  and  $n_{\text{out}}$  are the number of the inlet and outlet channels,  $w_{\text{ch,in}}$  and  $w_{\text{ch,out}}$  are the side lengths of the inlet and outlet channels, and  $l_{\text{DPF}}$  is the length of DPF.

## Model-based carbon load estimation

### Carbon load estimation overall design

As shown in the Figure 1, the carbon load estimation algorithm consists of two parts, the first part is the carbon load prediction based on the DPF model and the second part is the carbon load correction based on the measured pressure drop of the DPF. The carbon load prediction is first obtained from the exhaust gas state such as exhaust gas flow, particle concentration, DPF wall temperature, HC concentration and oxygen concentration, where the HC and oxygen concentrations are calculated from the DOC model (Wu et al. 2019). Due to the error accumulation during the iterative calculation process, an EKF is designed to eliminate the gradually accumulating error. The measured pressure drop data is used to correct the predicted values of carbon load. One-step prediction of the previously estimated value is obtained using the DPF model, and then the predicted value is updated based on the measured pressure drop data at the current time to obtain the estimated value of the current state.

### Design of extended Kalman filter

Since this DPF has an import/export ratio of 3:1,  $A_1 = 3A_2$ , introduce new variable  $c_1 = \frac{1}{c_{p,g1} \rho_{g1} n_{\text{in}} w_{\text{ch,in}}^2 l_{\text{DPF}}}$ ,  $c_2 = \frac{1}{c_{p,g2} \rho_{g2} n_{\text{out}} w_{\text{ch,out}}^2 l_{\text{DPF}}}$ ,  $c_3 = \frac{1}{c_{p,\text{DPF}} m_{\text{DPF}}}$ ,  $T'_w(k+1) = \exp\left[-\frac{E_c}{R_g T_w(k+1)}\right]$ ,  $T''_w(k+1) = \exp\left[-\frac{E_{\text{HC}}}{R_g T_w(k+1)}\right]$ ,  $A'_2 = A_2 h_2$ ,  $A_3 = A_2 \Delta H_C A_c$ ,  $A_4 = \Delta H_{\text{HC}} A_2 b_{\text{pt}} w_{\text{wall}} A_{\text{HC}}$ ,  $A_5 = \pi D_{\text{DPF}} l_{\text{DPF}} h_{\text{amb}}$ ,  $A_6 = 3A_2 M_{\text{particle}} A_c$

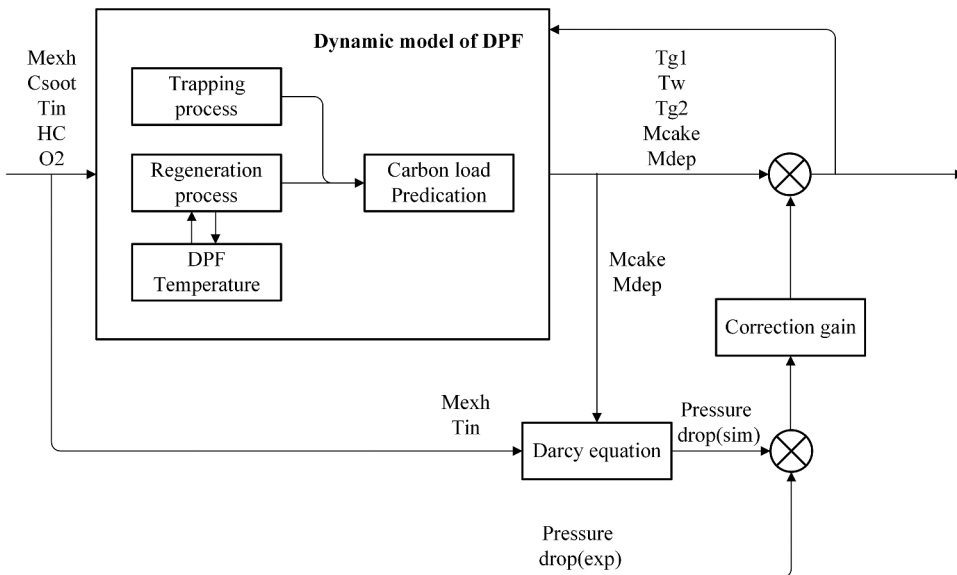


Figure 1. Overall process of carbon load estimation algorithm.

Considering  $T_{g1}(k)T_{g2}(k)T_w(k)m_{cake}(k)m_{dep}(k)$  as the state variables, The model is discretized as:

$$\begin{cases} \dot{T}_{g1}(k+1) = c_1 \{ \dot{m}_{exh}(k) c_{p,g1} [T_{in}(k) - T_{g1}(k)] + 3A'_2 [T_w(k) - T_{g1}(k)] \} \\ \dot{T}_{g2}(k+1) = c_2 \{ \dot{m}_{exh}(k) [c_{p,g1} T_{g1}(k) - c_{p,g2} T_{g2}(k)] + A'_2 [T_w(k) - T_{g2}(k)] \} \\ \dot{T}_w(k+1) = c_3 \{ A'_2 [3T_{g1}(k) + T_{g2}(k) - 4T_w(k)] \\ + A_3 C_{O_2}(k) T''(k+1) [3m_{cake}(k) + m_{dep}(k)] \\ + A_4 C_{O_2}(k) C_{HC}(k) T''_w(k+1) + A_5 [T_{amb} - T_w(k)] \} \\ \dot{m}_{cake}(k+1) = E_{cake} \frac{\dot{m}_{exh}(k)}{\rho_{exh}} C_{particle}(k) - 3A_6 C_{O_2}(k) m_{cake}(k) T'_w(k+1) \\ \dot{m}_{dep}(k+1) = E_{dep} (1 - E_{cake}) \frac{\dot{m}_{exh}(k)}{\rho_{exh}} C_{particle}(k) - A_6 C_{O_2}(k) m_{dep}(k) T'_w(k+1) \end{cases} \quad (27)$$

The state vector  $x(k) = [T_{g1}(k) \ T_{g2}(k) \ T_w(k) \ m_{cake}(k) \ m_{dep}(k)]^T$ , the input vector  $u(k) = [m_{exh}(k) C_{particle}(k) T_{in}(k) C_{HC}(k) C_{O_2}(k)]^T$ , measurement vector  $z(k) = P_{DPF}(k)$   $P_{DPF}$  is the pressure drop of DPF.

The DPF pressure drop consists of the pressure drop of clean DPF and the pressure drop due to particle trapping:

$$P_{DPF} = P_{clean} + P_{particle} = P_{fric1} + P_{fric2} + P_{con} + P_{expand} + P_{cake} + P_{dep} \quad (28)$$

$P_{clean}$  is the pressure drop of clean DPF,  $P_{particle}$  is the pressure drop caused by trapped particles,  $P_{fric1}$  and  $P_{fric2}$  are the pressure drops along the upstream and downstream flow paths of resistance,  $P_{con}$  and  $P_{expand}$  are the pressure drops caused by the contraction and expansion of the cross-section at the entrance and exit, and  $P_{cake}$  and  $P_{dep}$  are the pressure drops caused by cake layer and deep bed layer.

$P_{fric1}$  and  $P_{fric2}$  are calculated according to the Darcy-Weisbach Formula as follows:

$$P_{fric1} = \frac{16\mu_{g1} U_1 l_{DPF}}{w_{ch,in}^2} \quad (29)$$

$$P_{fric2} = \frac{16\mu_{g2} U_2 l_{DPF}}{w_{ch,out}^2} \quad (30)$$

$\mu_1$  and  $\mu_2$  are the air viscosity in the inlet and outlet channels,  $U_1$  and  $U_2$  are the upstream and downstream flow rates.

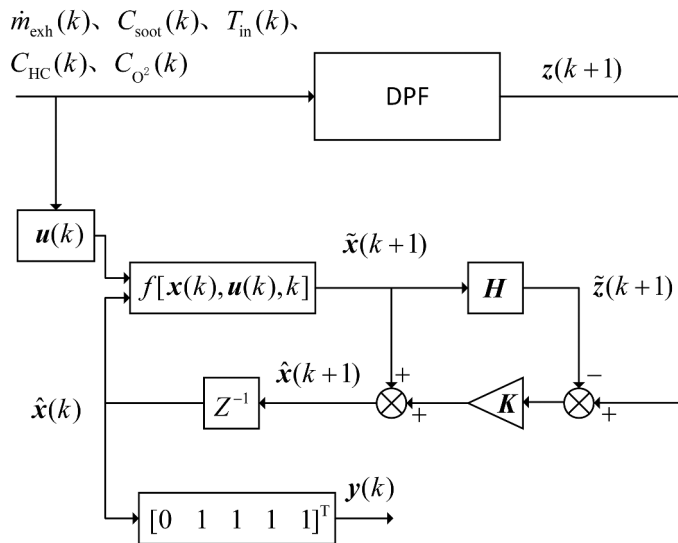


Figure 2. Schematic diagram of EKF recurrence algorithm.



$P_{\text{con}}$  and  $P_{\text{expand}}$  are calculated as follows:

$$P_{\text{con}} = \frac{1}{2} \rho_{g1} \xi U_1^2 \quad (31)$$

$$P_{\text{expand}} = \frac{1}{2} \rho_{g2} \xi U_2^2 \quad (32)$$

$\rho_{g1}$  and  $\rho_{g2}$  are the density of upstream and downstream gas,  $\xi$  is the expansion and contraction coefficient, generally taken as 0.82.

In the process of particle accumulation, the pressure drop caused by the cake layer trapping accounts for the main part, to simplify the calculation, the deep bed and the cake layer particles are unified as the cake layer:

$$P_{\text{cake}} + P_{\text{dep}} = \frac{\mu_{\text{gw}}}{k_{\text{cake}}} w_{\text{particle}} u_w \quad (33)$$

$\mu_{\text{gw}}$  is the air viscosity in the porous wall,  $k_{\text{cake}}$  is the permeability of the cake layer,  $w_{\text{particle}}$  is the equivalent cake layer particle accumulation thickness,  $u_w$  is the velocity of gas inside the porous wall.

The conversion relationship between  $w_{\text{particle}}$  and  $m_{\text{particle}}$  is:

$$w_{\text{particle}} = \frac{m_{\text{particle}}}{4n_{\text{in}} w_{\text{ch,in}} l_{\text{DPF}} \rho_{\text{particle,cake}}} \quad (34)$$

$\rho_{\text{particle,cake}}$  is the particle density in the cake layer.

The cake layer permeability is calculated according to previous studies (Wu et al. 2019), using a modified form of slip factor with the following equation.

$$k_{\text{cake}} = SCF \cdot k_{\text{con}} \quad (35)$$

$k_{\text{con}}$  is the slip-free permeability of the cake layer without considering the effect of slip in the cake layer,  $SCF$  is the Stokes-Cunningham slip correction factor, for which the corresponding formula is given according to the literature (Chiavola et al. 2020).

$$SCF = 1 + Kn(1.257 + 0.4e^{-\frac{1}{Kn}}) \quad (36)$$

$Kn$  is the Knudsen number.

$$Kn = \frac{2\lambda}{d_p} \quad (37)$$

$$\lambda = \frac{\mu_g}{\rho_g} \sqrt{\frac{\pi M_{\text{air}}}{2R_g T_w}} \quad (38)$$

$\lambda$  is the mean free range of the gas molecules,  $M_{\text{air}}$  is the molar mass of air, and  $R_g$  is the molar gas constant.

Therefore, the measurement vector  $z(k) = P_{\text{clean}} + \frac{\mu_{\text{gw}}}{k_{\text{cake}}} u_w \frac{m_{\text{cake}}(k) + m_{\text{dep}}(k)}{A_1 \rho_{\text{particle,cake}}}$ , let  $A_6 = \frac{\mu_{\text{gw}}}{k_{\text{cake}}} u_w \frac{1}{A_1 \rho_{\text{particle,cake}}}$ , measurement output vector  $H = [000A_6A_6]^T$ . Introduce the state noise vector  $w(k) \sim N(0, Q(k))$  to compensate for errors caused by variation and discretization of the model parameters with operating conditions; introduce the measurement noise vector  $v(k) \sim N(0, R(k))$  to compensate for random disturbances in DPF pressure drop measurements. The corresponding system equation of state and measurement equation becomes:

$$\begin{cases} x(k+1) = f[x(k), u(k), k] + w(k) \\ z(k) = P_{\text{clean}} + Hx(k) + v(k) \end{cases} \quad (39)$$

### Design of extended Kalman filter -based carbon load state observer

A diagram of the EKF-based carbon load state observer is given in Figure 2 below

The inputs to the carbon load state observer are the DPF inlet temperature  $T_{\text{in}}(k)$ , the exhaust particulate concentration  $C_{\text{particle}}(k)$ , and the exhaust mass flow  $\dot{m}_{\text{exh}}(k)$ .

The output of the carbon load state observer is:

$$y(k) = [0 \hat{T}_{g2}(k) \hat{T}_w(k) \hat{m}_{\text{cake}}(k) \hat{m}_{\text{dep}}(k)]^T \quad (40)$$

## DPF carbon load estimation verification

### Experimental setup

To validate the DPF dynamic model and carbon load estimation method, DPF trapping and regeneration experiments were conducted. The test adopted a 3.0 L displacement diesel engine provided by a domestic manufacturer, and the main parameters of the diesel engine are shown in Table 1. The diesel engine was speed-torque balanced with an electric dynamometer to produce exhaust gases at different operating conditions as input, which was equipped with pressure and temperature sensors to monitor its operation. The exhaust gases generated at different operating conditions are used as input to the after-treatment system.

The overall structure of the test is shown in Figure 3. The hydrocarbon nozzle was mounted at the front end of the DOC, and the exhaust gas temperature sensor and mass flow sensor were arranged after the diesel exhaust gas turbocharger. The temperature sensors were high-temperature resistant K-type armored thermocouples with 1 mm diameter. T2-T5 were the temperature sensors associated with the DPF, arranged in positions corresponding to the inlet, inside and the outlet of the DPF. Thermocouples inside the DPF were tightly fitted to the DPF carrier, and the measured temperatures were recorded as  $T_{w1}$ ,  $T_{w2}$  and  $T_{w3}$ , which were weighted and averaged to obtain the average wall temperature of the DPF,  $T_w$ . The two pins of the DPF pressure sensor were respectively connected to the inlet of the DPF and the outlet of the DPF to measure the pressure drop between the DPF inlet and outlet.

A PegasorMi2 particle analyzer was used to measure the concentration of particles in the diesel engine at all steady state conditions. According to the particle concentration data, we chose the condition with a large flow rate, fast carbon accumulation, and airflow temperature below 300°C to do the carbon loading accumulation, and the test at the condition of 2800 r/min-94 N·m met the requirements. The loading of 5–8 hours could reach the regeneration carbon loading at one time. The pressure drop data were measured while loading. The regeneration test was conducted in open-loop injection mode, a fixed steady state condition was selected, diesel was injected before DOC to heat the exhaust gas, and the DPF inlet temperature was maintained in the range of 500–600°C, and the pressure drop and the temperature change of each point were recorded during the regeneration process.

### Model parameters identification

Parameters related to the DPF structure are provided by the manufacturer, as shown in Table 2.

The parameters that were not calibrated were  $k_{\text{con}}$ ,  $k_{\text{dep0}}$ ,  $\rho_{\text{particle,dep}}$ ,  $\rho_{\text{particle,cake}}$ ,  $d_p$ ,  $\varphi$ ,  $A_c$ , and  $E_c$ . The first six parameters were calibrated by the changes in the pressure drop during the trapping process. The fast trapping condition of 2800 r/min-94 N·m and the idle condition of 800 r/min-0 N·m were selected for the calibration parameters. The calibration features were mainly selected from the starting pressure drop of the clean DPF, the slope of the pressure drop growth in the deep bed trapping stage, the turning

**Table 1.** Engine parameters.

Item	Parameter
Type	L4
Stroke	95mm
Bore	105mm
Rated power	115kW(3200rpm)
Max torque	400Nm
Injection system	Common rail
Emission level	China V

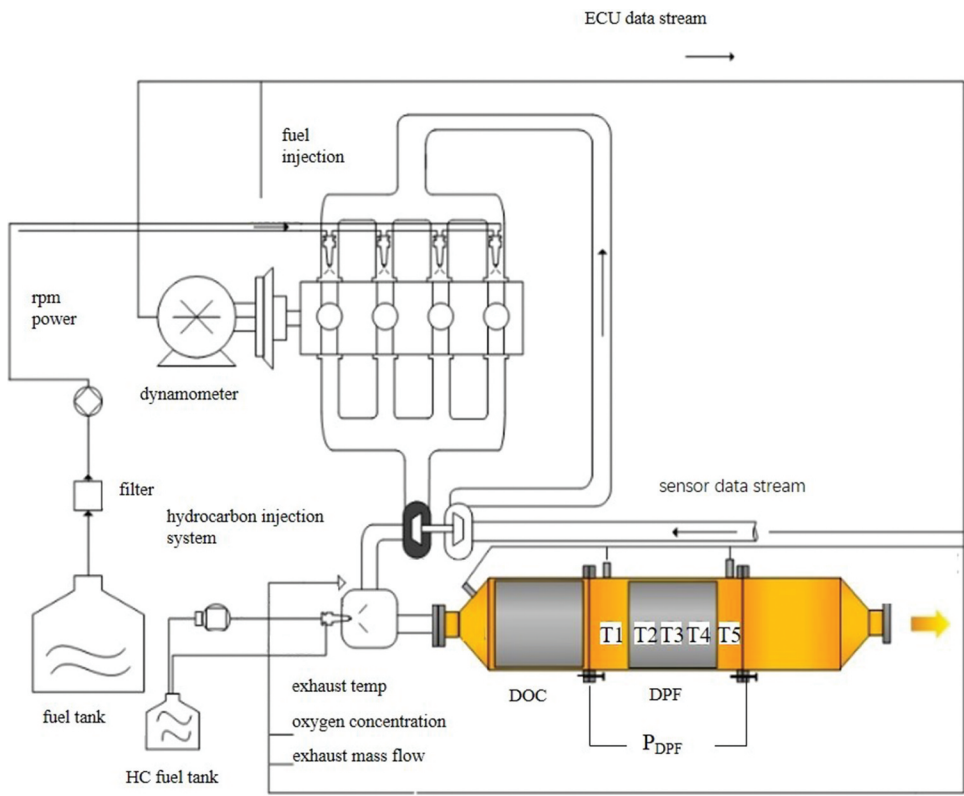


Figure 3. Schematic diagram of the engine bench.

point of the transition from deep bed to cake layer trapping, and the slope of the pressure drop growth due to the cake layer trapping after the turning. The parameters are shown in Table 3.

The wall temperature data during regeneration of 5 g/L carbon load at 1300 r/min-220 N·m and 8 g/L carbon load at 1300 r/min-216 N·m was collected to calibrate  $A_c$  and  $E_c$ . The calibrated model parameters related to the trapping flow are shown in Table 4.

### Carbon load estimation verification

Figure 4 shows the simulated and experimental curves of wall temperature, pressure drop, and carbon load estimates for DPF trapping to 5 g/L carbon load at 2800 r/min – 84 NM load condition:

Table 2. DPF parameter.

Item	Parameter
$d_{DPF} \times l_{DPF}$	$190.5 \times 127\text{mm}$
$m_{DPF}$	2.677kg
material	SiC
Cells	300cpsi
$\epsilon_0$	0.42
$w_{wall}$	0.254mm
$n_{in}$	9936
$n_{out}$	3312
$n_{dep}$	$4.8836 \times 10^{-14}$
$w_{ch,in} = w_{ch,out}$	0.0012m
$h_1=h_2$	20 W/(m <sup>2</sup> · K)
$h_{amb}$	10 W/(m <sup>2</sup> · K)

**Table 3.** Trap relevant related parameters.

Parameter	Value
$k_{\text{con}}$	$1.45 \times 10^{-14} \text{m}^2$
$k_{\text{dep0}}$	$5.4 \times 10^{-12} \text{m}^2$
$\rho_{\text{particle,dep}}$	$8.15 \text{kg/m}^3$
$\rho_{\text{particle,cake}}$	$121.6 \text{kg/m}^3$
$d_p$	$5.0 \times 10^{-6} \text{m}$
$\varphi$	0.9

**Table 4.** Regeneration related parameters.

Parameter	Value
$A_c$	$1.5 \times 10^7$
$E_c$	$1.2 \times 10^5 \text{J/mol}$
$A_{\text{HC}}$	$1.9 \times 10^{25}$
$E_{\text{HC}}$	$2.01 \times 10^5 \text{J/mol}$

It can be seen that the trajectory of pressure drop in the trapping stage is typical of three trapping stages, in 0-1000s, the DPF is in the process of deep-bed trapping, in 1000–2000s, it is in the excessive stage of deep-bed trapping to cake-layer trapping, and it is in the stage of cake-layer trapping after 2000s. The maximum error of the simulation model is less than 0.7kPa and the average error is less than 0.23kPa. The temperature in the DPF during the trapping process is basically kept constant. The carbon load prediction is shown in Figure 4. The carbon load calculated based on the pressure drop under the steady state condition is used as a reference. It can be seen that the maximum error of the carbon load prediction is 0.3 g/L, and the average error is less than 0.17 g/L. Despite the smoothing measures taken for the pressure drop, there were still apparent fluctuations in the carbon load calculated based on the pressure drop, and when a large change in the operating conditions occurs at about 17,000 s, the carbon load calculated based on the pressure drop drastically fluctuates and distorts, which also illustrates the advantages of model-based carbon load prediction.

The simulated and experimental curves of the estimated DPF wall temperature, pressure drop, and carbon load during the dynamic regeneration of a DPF with a trapped carbon load of 5 g/L are presented in Figure 5. The operating condition is shown in Figure 6:

It can be seen that the pressure drop in the regeneration stage changes with the engine speed. 0-200s, the engine speed first decreases, the pressure drop also decreases, and then pressure drop increases due to the increase of DPF temperature. After that, from 200-900s, the change of pressure drop is consistent with the trend of engine speed. After 900s, the pressure drop also decreases due to the decrease of DPF temperature. Throughout the process, the maximum error of the model pressure drop does not exceed 0.7kPa, and the average error does not exceed 0.33kPa. The temperature change is caused by the injection of diesel fuel in front of the DOC at 0 s. The DPF wall temperature gradually rises from 600 K to 920 K from 0 s to 200 s. During this period, the temperature increase in particle regeneration overlaps with the temperature increase from hydrocarbon oxidation, which then slowly increases to 970 K. The hydrocarbon nozzle stops injecting diesel fuel after about 800 s, and the DPF temperature gradually decreases to 600 K. The maximum error of the model temperature is less than 0.33 kPa. The maximum error of the modeled temperatures is less than 90 K, and the average error does not exceed 50 K. The carbon load depletion rate is low at the beginning of regeneration due to the low wall temperature, and then accelerates when the wall temperature rises at 150 s. At 800 s, the carbon load tends to zero and the DPF regeneration is basically complete.

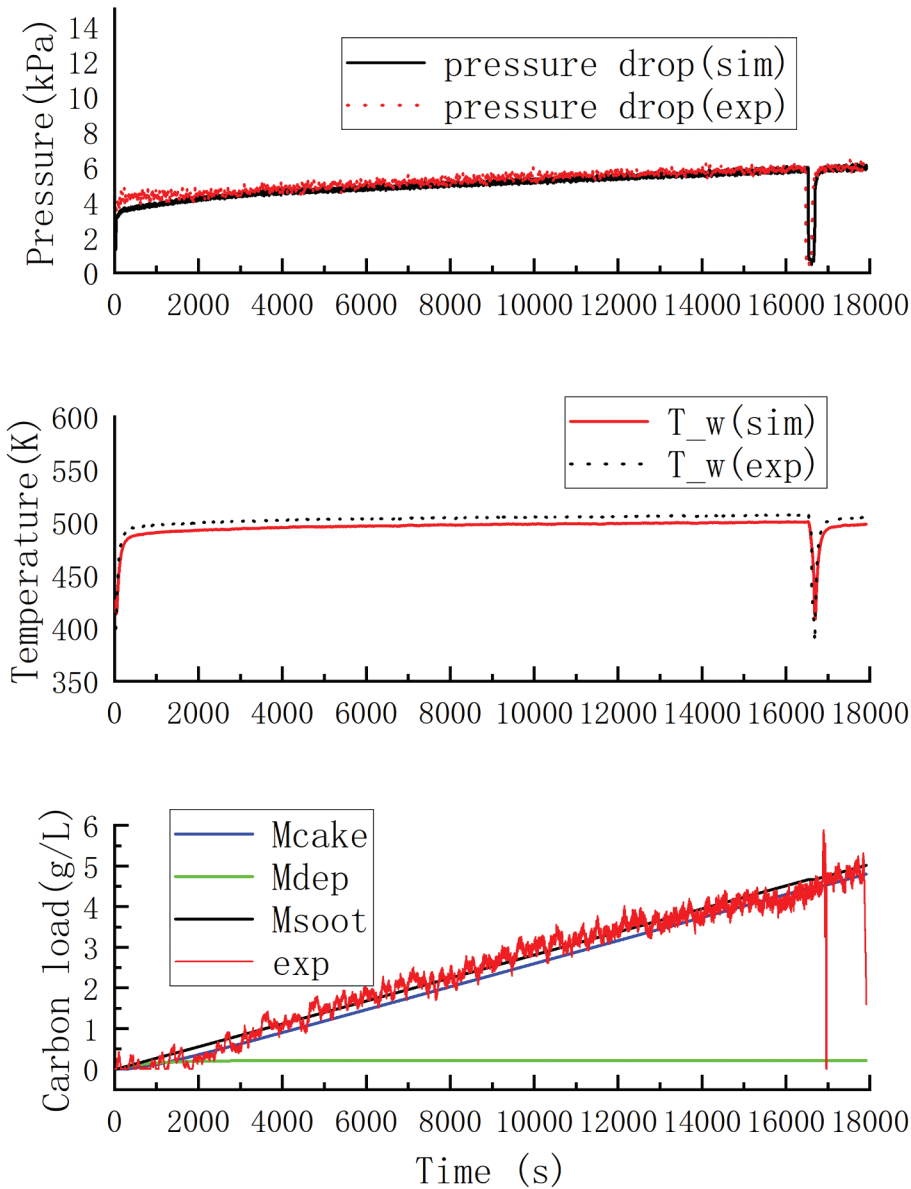


**Figure 4.** Simulated and experimental comparison of the fast trapping process.

For carbon loading prediction and DPF pressure drop, the model reflects the experimental results well, and the error mainly comes from the numerical fluctuation of the pressure drop sensor itself. The error of DPF temperature is larger in the process of temperature rise and fall, one side is due to the temperature change of DPF in the axial direction, the average temperature of the three thermocouples is different from the wall temperature in the model; on the other hand, the DPF carrier has heat capacity, and the model does not take this into account, so the temperature rise and fall of the simulation will be faster than the actual one. DPF temperature is mainly used in the design of the regeneration strategy to ensure that the DPF is at a safe temperature with a certain margin, so a slightly larger error is acceptable.

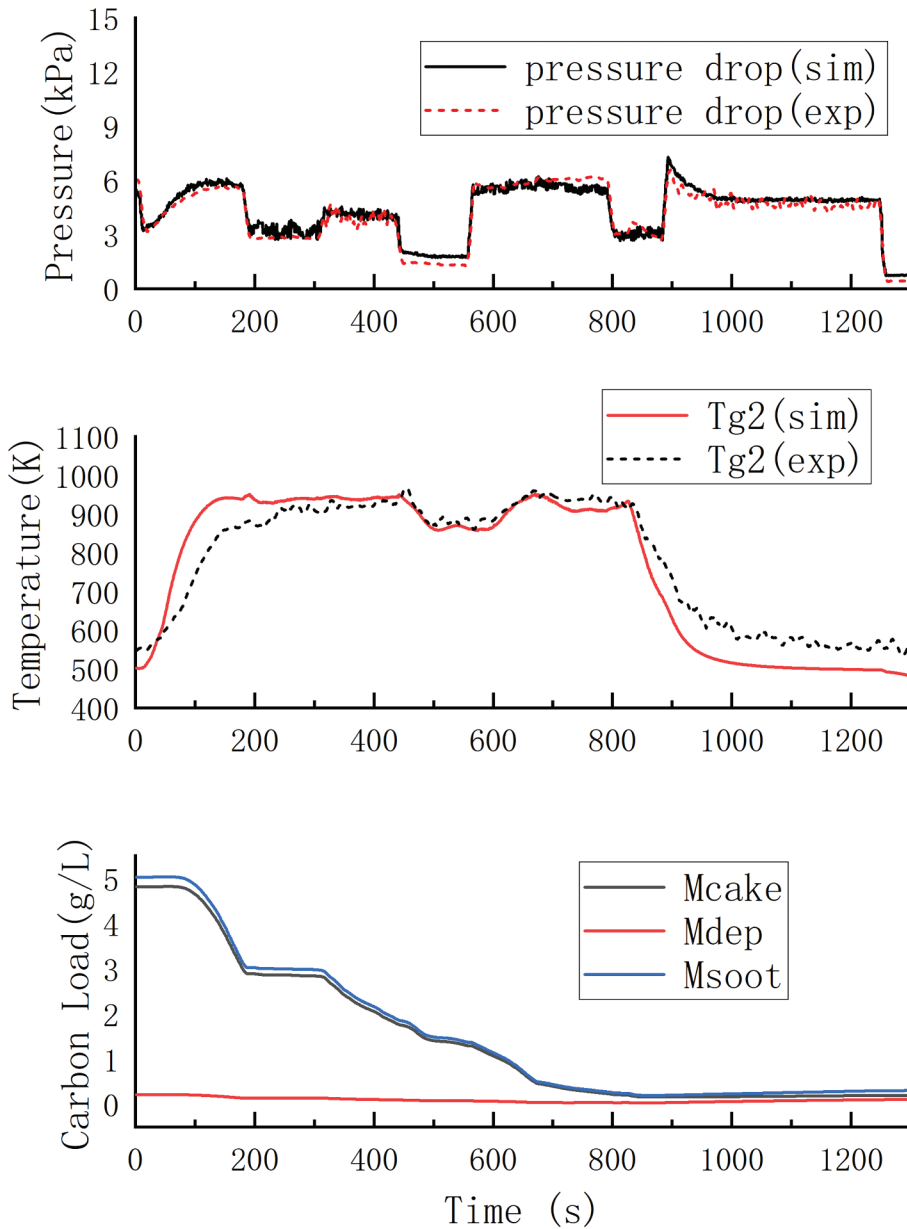


**Figure 5.** Simulated and experimental comparison of the dynamic regeneration process.

The model can well reflect the parameter changes during DPF trapping and regeneration process in both steady state and dynamic operating conditions. The carbon load estimation algorithm can achieve accurate prediction of carbon load during DPF trapping and regeneration, which can be used to judge the start and stop of DPF regeneration. The prediction of DPF pressure drop and wall temperature under variable operating conditions can be used to monitor the parameter changes during the operation of DPF, in particular, to ensure that the regeneration is carried out safely and effectively.

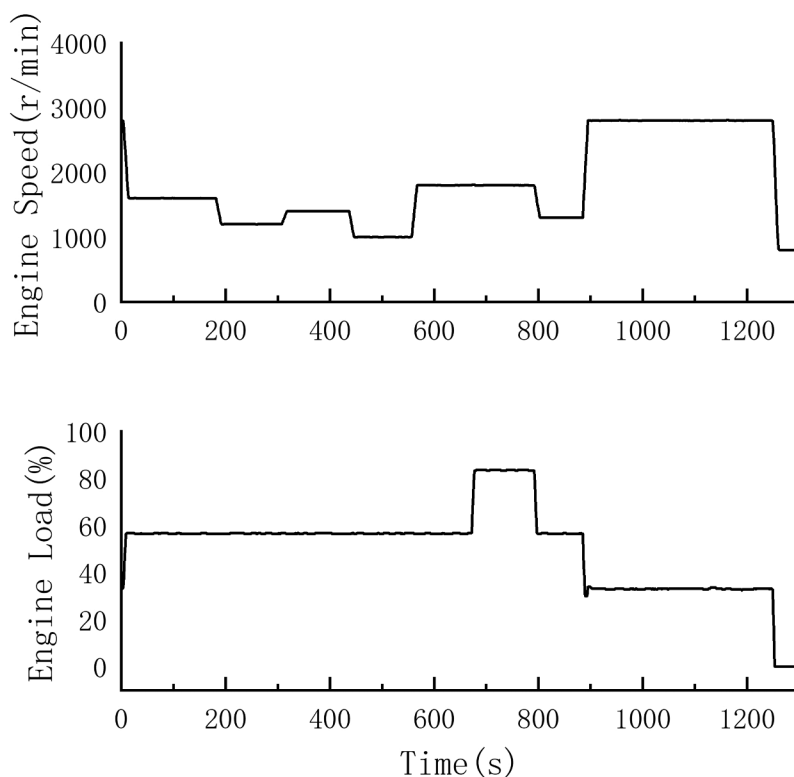


**Figure 6.** Operating condition of DPF dynamic regeneration.

## Conclusion

In this paper, a simplified model of the DPF capture and regeneration process was established, and based on the DPF model, the carbon load prediction was corrected by adding the DPF pressure drop. The aim is to predict the particle loading during DPF loading and regeneration under actual engine operation for the control and optimization of active DPF regeneration.

The above model and carbon load estimation algorithm were validated by DPF capture and regeneration experiments. The maximum error of carbon load prediction was 0.3 g/L, and the average error was less than 0.17 g/L. The maximum error of pressure drop was 0.7kPa, and the average error was less than 0.33kPa, the maximum error of the wall temperature was less than 90 K, and the average error didn't exceed 50 K. The model can well reflect the changes in carbon load and pressure drop during DPF capture and regeneration and shows good accuracy, which can be used to predict the variation of carbon loading under different engine operating conditions, so as to achieve the optimal control strategy for DPF regeneration to ensure high filtration efficiency, reduce the fuel consumption of frequent regeneration. Predicted pressure drop and temperature can be used to monitor DPF operation and ensure the safety of the DPF.

More intensive research will be carried out in this work in the future, where the model can be used to study the regeneration of DPF under different inlet conditions (e.g., temperature, oxygen concentration, exhaust gas flow rate, etc.) to optimize the control of active regeneration of DPF. It makes sense to further improve the accuracy of the DPF model without significantly increasing the computational burden. SCR catalyst-coated DPF will be used in the future after-treatment system, so the study of the trapping and regeneration process of the SCR catalyst-coated DPF is necessary.

## Abbreviations

DOC Diesel oxidation catalyst

DPF	Diesel particulate filters
ECU	Electronic Control Unit
EKF	Extended Kalman filter
HC	Hydrocarbon
PM	Particulate matter
PN	Particulate number
SCF	Stokes-Cunningham slip correction factor
SCR	Selective catalytic reduction

## Disclosure statement

No potential conflict of interest was reported by the author(s).

## Funding

This study was financially supported by the National Key R&D Program of China (Grant No. 2022YFE0209000) and the National Natural Science Foundation of China (Grant No. 52176135 and 52276136).

## Notes on contributors

**Dongwei Yao** was born in Deqing, Zhejiang, China, in 1981. He received the B.S. degree in vehicle engineering and the Ph.D. degree in power machinery and engineering from Zhejiang University, Zhejiang, China, in 2005 and 2010, respectively. In 2010, he became an Assistant Professor and also Postdoctoral Fellow with the College of Energy Engineering, Zhejiang University. From 2014 to 2015, he was a Visiting Scholar and Research Assistant with the University of Illinois at Urbana-Champaign, Champaign, IL, USA. Since 2017, he has been an Associate Professor with the College of Energy Engineering, Zhejiang University. He has authored or coauthored more than 30 articles, and attained more than 25 inventions. His research interests include engine combustion and emission control, electrical and hybrid electrical vehicle control.

**Jiadong Hu** received the B.S. degree in vehicle engineering from Zhejiang University, Zhejiang, China, in 2020. He is currently working toward the Ph.D. degree in power machinery and engineering thermophysics with the College of Energy and Power Engineering, Zhejiang University, Zhejiang, China.

**Benxi Zhang** received the B.S. degree in vehicle engineering and the Ph.D. degree in power machinery and engineering from Zhejiang University, Zhejiang, China, in 2014 and 2021, respectively.

**Yihe Zhang** received the B.S. degree in vehicle engineering from Shandong University, Shandong, China, in 2022. He is currently working toward the Ph.D. degree in power machinery and engineering thermophysics with the College of Energy and Power Engineering, Zhejiang University, Zhejiang, China.

**Feng Wu** received the B.S. and Ph.D. degrees in internal combustion engine from Zhejiang University, Zhejiang, China, in 1990 and 1996, respectively. In 1996, he became a Lecturer with the Department of Energy Engineering, Zhejiang University. From 1998 to 2006, he was an Associate Professor in the same department. Since 2006, he has been a Full Professor with the College of Energy Engineering, Zhejiang University. He has authored or coauthored more than 50 articles, and attained more than 25 inventions. His research interests include engine combustion and emission control, engine clean alternative fuels, electrical and hybrid electrical vehicle control.

## References

- Bai, S., J. Tang, G. Wang, and G. Li. **2016a**. Soot loading estimation model and passive regeneration characteristics of DPF system for heavy-duty engine. *Applied Thermal Engineering* 100:1001292–98. doi:[10.1016/j.applthermaleng.2016.02.055](https://doi.org/10.1016/j.applthermaleng.2016.02.055).
- Bai, S., J. Tang, G. Wang, and G. Li. **2016b**. Soot loading estimation model and passive regeneration characteristics of DPF system for heavy-duty engine. *Applied Thermal Engineering* 100:1292–98. doi:[10.1016/j.applthermaleng.2016.02.055](https://doi.org/10.1016/j.applthermaleng.2016.02.055).
- Bin, G., Z. Reggie, L. He, and H. Zhen. **2015**. Review of the state-of-the-art of exhaust particulate filter technology in internal combustion engines. *Journal of Environmental Management* 154:225–58. doi:[10.1016/j.jenvman.2015.02.027](https://doi.org/10.1016/j.jenvman.2015.02.027).
- Chiavola, O., G. Chiatti, D. M. Cavallo, et al. Modeling of soot deposition and active regeneration in wall-flow DPF and experimental Validation[R]. SAE Technical Paper, 2020.



- Chiavola, O., G. Chiatti, and N. Sirhan. 2019. Impact of particulate size during deep loading on DPF management. *Applied Sciences* 9 (15):3075. doi:10.3390/app9153075.
- Depcik, C., C. Langness, J. Mattson Development of a simplified diesel particulate filter model intended for an engine control unit[R]. SAE Technical Paper, 2014.
- Di Sarli, V., and A. Di Benedetto. 2015. Modeling and simulation of soot combustion dynamics in a catalytic diesel particulate filter. *Chemical Engineering Science* 137:69–78. doi:10.1016/j.ces.2015.06.011.
- Di Sarli, V., and A. Di Benedetto. 2016. Operating map for regeneration of a catalytic diesel particulate filter. *Industrial & Engineering Chemistry Research* 55 (42):11052–61. doi:10.1021/acs.iecr.6b02521.
- Di Sarli, V., and A. Di Benedetto. 2018. Combined effects of soot load and catalyst activity on the regeneration dynamics of catalytic diesel particulate filters. *AIChE Journal* 64 (5):1714–22. doi:10.1002/aic.16047.
- Di Sarli, V., and A. Di Benedetto. 2019. Using CFD simulation as a tool to identify optimal operating conditions for regeneration of a catalytic diesel particulate filter. *Applied Sciences* 9 (17):3453. doi:10.3390/app9173453.
- Du, Y., G. Hu, S. Xiang, K. Zhang, H. Liu, and F. Guo. 2018. Estimation of the diesel particulate filter soot load based on an equivalent circuit model. *Energies* 11 (2):472. doi:10.3390/en11020472.
- Feulner, M., F. Seufert, A. Müller, G. Hagen, and R. Moos. 2017. Influencing parameters on the microwave-based soot load determination of diesel particulate filters. *Topics in Catalysis* 60 (3–5):374–80. doi:10.1007/s11244-016-0626-7.
- Huang, T., G. Hu, F. Guo, and Y. Zhu. 2019. Investigation of a model-based approach to estimating soot loading amount in catalyzed diesel particulate filters. *SAE International Journal of Engines* 12 (5):567–78. doi:10.4271/103-12-05-0036.
- Jin, M., L. Tian, and J. Tong. 2016. A meta-analysis of the effect of atmospheric PM10 pollution on population mortality in China. *Journal of Environment and Health*. 33 (008):725–729. doi:10.16241/j.cnki.1001-5914.2016.08.018.
- Kort, A., F. X. Ouf, T. Gelain, J. Malet, R. Lakhmi, P. Breuil, and J.-P. Viricelle. 2021. Quantification of soot deposit on a resistive sensor: Proposal of an experimental calibration protocol. *Journal of Aerosol Science* 156:105783. doi:10.1016/j.jaerosci.2021.105783.
- Landi, G., V. Di Sarli, and L. Lisi. 2021. A numerical investigation of the combined effects of initial temperature and catalyst activity on the dynamics of soot combustion in a catalytic diesel particulate filter. *Topics in Catalysis* 64 (3–4):270–87. doi:10.1007/s11244-020-01386-w.
- Lao, C., J. Akroyd, N. Eaves, A. Smith, N. Morgan, A. Bhavé, and M. Kraft. 2019. Modelling particle mass and particle number emissions during the active regeneration of diesel particulate filters. *Proceedings of the Combustion Institute* 37 (4):4831–38. doi:10.1016/j.proci.2018.07.079.
- Ran, Y., T. Huang, M. Zhang, S. Jing, and Y. Zhu. 2018. DPF soot loading estimation strategy based on pressure difference. *IFAC-Papersonline* 51 (31):366–68. doi:10.1016/j.ifacol.2018.10.075.
- Reşitoğlu, İ. A., K. Altınışık, and A. Keskin. 2015. The pollutant emissions from diesel-engine vehicles and exhaust aftertreatment systems. *Clean Technologies and Environmental Policy* 17 (1):15–27. doi:10.1007/s10098-014-0793-9.
- Rossomando, B., I. Arsie, E. Meloni, et al. Experimental test on the feasibility of passive regeneration in a catalytic DPF at the exhaust of a light-duty diesel engine[R]. SAE Technical Paper, 2019.
- Shi, Y., Y. Cai, X. Li, X. PU, N. ZHAO, and W. WANG. 2019. Effect of the amount of trapped particulate matter on diesel particulate filter regeneration performance using non-thermal plasma assisted by exhaust waste heat. *Plasma Science and Technology* 22 (1):015504. doi:10.1088/2058-6272/ab4d3c.
- Shi, X., D. Jiang, Y. Liang, and P. Liang. 2020. Research on carbon load prediction model of DPF based on circulation resistance. *Automotive Engineering* 42 (9):1183–88.
- Sun, Y., T. Cai, and D. Zhao. 2021. Thermal performance and NOx emission characteristics studies on a premixed methane-ammonia-fueled micro-planar combustor. *Fuel* 291:120190. doi:10.1016/j.fuel.2021.120190.
- Tang J., G. Li, and Z. Wang. 2015. Construction and experiment of DPF soot loading model. *Transactions of Csice* 33 (1):51–57. doi:10.16236/j.cnki.nrjxb.201501008.
- Tan, P., D. Wang, C. Yao, L. Zhu, Y.-H. Wang, M.-H. Wang, Z.-Y. Hu, and D.-M. Lou. 2020. Extended filtration model for diesel particulate filter based on diesel particulate matter morphology characteristics. *Fuel* 277:118150. doi:10.1016/j.fuel.2020.118150.
- Wang, D. 2013. Research on diesel particle trap and its regeneration Technology. Jilin University. <https://kns.cnki.net/kcms2/article/abstract?v=O9dCEmDP74LANvTEr7KNGOuFRumcCvjHXTE1XJ0RnIKVdGmkeTPmK2U73mB7Qj-6nYvYhYAfmF2GjUwcZs3ZroUuNynSG3dYiR745-aGXviKqDi0UTNxA6KzMp8-K-AnV9ozwGFd7YmM27qqLZmH5Q==&uniplatform=NZKPT&language=CHS>
- Wang, D., P. Tan, L. Zhu, Y.-H. Wang, Z.-Y. Hu, and D.-M. Lou. 2021. Novel soot loading prediction model of diesel particulate filter based on collection mechanism and equivalent permeability. *Fuel* 286:119409. doi:10.1016/j.fuel.2020.119409.
- Wu, F., B. Zhang, D. Yao, and Y. Yang. 2019. Modeling and order reduction for the thermodynamics of a diesel oxidation catalyst with hydrocarbon dosing. *Catalysts* 9 (4):369. doi:10.3390/catal9040369.
- Zhang, B., H. Zuo, Z. Huang, J. Tan, and Q. Zuo. 2020. Endpoint forecast of different diesel-biodiesel soot filtration process in diesel particulate filters considering ash deposition. *Fuel* 272:117678. doi:10.1016/j.fuel.2020.117678.
- Zhong, C., J. Liang, Y. Zhu, H. Zuo, S. Wang, B. Chen, X. Wu, and C. Wu. 2022. Effects analysis on soot oxidation performance in the diesel particulate filter based on synergetic passive-active composite regeneration methods. *Chemical Engineering Science* 262:118013. doi:10.1016/j.ces.2022.118013.